Research Article

Investigation of energy band-gap of the composite of hexaferrites and polyaniline

T. Tchouank Tekou Carol[1] · Amar Srivastava[1] · J. Mohammed[1,2] · Shaweta Sharma[1] · G. Mukhtar[1,3] · A. K. Srivastava[1]

Received: 21 November 2019 / Accepted: 13 March 2020 / Published online: 9 April 2020

Abstract
The Bi–Al doped M-type hexaferrite ($BaFe_{11.8}Bi_{0.1}Al_{0.1}O_{19}$) was prepared by the use of sol gel auto combustion process. The prepared sample was sintered at 1000 °C for 5 h. Polyaniline was synthesized by oxidative polymerization. Mechanical blending was used to synthesize $BaFe_{11.8}Bi_{0.1}Al_{0.1}O_{19}$-PANI composite. X-ray diffraction (XRD), Fourier Transform Infra-red spectroscopy (FTIR), Field Emission Scanning Electron Microscope, Energy Dispersive X-ray spectroscopy and UV–vis-NIR spectroscopy were used for structural and optical analysis. XRD spectra show pure single phase of M-type hexagonal ferrites. The presence of bands in FTIR spectra in the range of 400–600 cm^{-1} and 800–1600 cm^{-1} indicate possible formation of hexaferrite and PANI. The band gaps were found nearly 2.24, 2.36 and 2.21 eV for HP1, HP2 and HP3 respectively.

Keywords M-type hexaferrite · Polyaniline · Absorbance · Band gap

1 Introduction

Hexaferrites materials are ferromagnetic materials that have a hexagonal crystal structure. These materials retained a great attention of the scientific community because of their excellent magnetic properties. Due to this reason, they are very useful in many applications such as supercapacitors, permanent magnets, microwave absorbing, medicine, magnetic recording and refrigerator magnets [1–3]. M-type barium hexaferrite shows a saturation magnetization of 72 emu/g and coercive field of 6700 Oe [4]. However, the magnetic properties of M-type hexaferrite can be modified by substituting a host element. In our previous work, we synthesized Al–Cr substituted M-type barium hexaferrite $BaFe_{12-2x}Al_xCr_xO_{19}$ ($x = 0.0$, 0.2, 0.4) where samples with $x = 0.0$ and $x = 0.4$ showed a saturation magnetization of 81.25 and 88.03 emu/g respectively whereas that of $x = 0.2$ showed 15.16 emu/g [5]. It was reported that variation in saturation of magnetization depends on occupancy of ferric crystallographic sites (2a, 2b, $4f_1$, $4f_2$ and 12k) [5]. Out of magnetic properties of M-type hexaferrite materials, their optical properties were also studied. The optical band gap values of $Ba_{1-x}Zn_xFe_{12}O_{19}$ ($0.0 \le x \le 0.3$) were found to be in the range 1.69–1.76 eV [6]. These band gap values are very comparable to those of single junction solar cell [7].

Polymers also called macromolecules are organic compounds composed of repeated subunits called monomers. They are generally known for their physical properties (softness, low density) and their insulating character. However, conductive polymers are so particular than others because of their π-conjugated bond which attribute them interesting electrical properties. Due to those electrical properties, conducting polymers are used in many applications such as electro-chromic smart windows, rechargeable batteries, sensors, antistatic coating, corrosion inhibitors, electronic, EMI shielding, supercapacitors and electrodes [8–13]. Inside the great family of

✉ A. K. Srivastava, srivastava_phy@yahoo.co.in; T. Tchouank Tekou Carol, ttctcadel@gmail.com | [1]Department of Physics, Lovely Professional University, Phagwara 144411, Punjab, India. [2]Department of Physics, Faculty of Science, Federal University Dutse, P.M.B. 7156, Dutse, Jigawa State, Nigeria. [3]Department of Science Education, Faculty of Arts and Education, Bauchi State University, Gadau, P.M.B. 65, Itas/Gadau, Bauchi State, Nigeria.

conducting polymers, there are polypyrrole, polyaniline, polythiophene, etc. Among these polymers, polyaniline (PANI) retained great attention because of more advantages such as low cost and easy synthesis, good environmental and chemical stability, tunable properties and availability of raw materials [13]. PANI is generally used as matrix in the synthesis of composites.

Several investigators combined these magnetic materials with others and many characterizations such as magnetic, dielectric and microwave absorption properties have been done [14–17]. Different methods were used to prepare nanoparticles including co-precipitation technique, glass-crystallization, aerosol pyrolysis, ceramic process, gel self-combustion method and sol–gel method [18–24]. In this present work, Bi–Al doped M-type barium hexaferrite with chemical formula $BaFe_{11.8}Bi_{0.1}Al_{0.1}O_{19}$ and PANI were prepared separately using sol gel method and oxidative polymerization respectively and the effect of PANI on optical properties of M-type hexaferrite $BaFe_{11.8}Bi_{0.1}Al_{0.1}O_{19}$ was investigated.

2 Experimental methods

2.1 Synthesis method of $BaFe_{11.8}Bi_{0.1}Al_{0.1}O_{19}$

Sol- gel method was employed to make $BaFe_{11.8}Bi_{0.1}Al_{0.1}O_{19}$ powder. Initially, raw chemicals with high purity (98–99.5%) such as $Ba(NO_3)_2$ (Loba chemistry), $Fe(NO_3)_3{\cdot}9H_2O$ (Loba chemistry), $Al(NO_3)_3{\cdot}9H_2O$ (Loba chemistry) $Bi(NO_3)_3{\cdot}5H_2O$ (CDH), ethylene glycol ($C_2H_6O_2$) (Loba chemistry) and citric acid ($C_6H_8O_7.H_2O$) (Loba chemistry) were used as starting materials. Then, after an appropriate stoichiometric measurement of each metal nitrate, the set was poured in 50 mL of ethylene glycol used as solvent. The set of starting materials was dissolved in 50 mL of ethylene glycol. Citric acid was added as a fuel in the ratio 1:1.5 with cations. Then, the neutral solution was obtained by adding of ammonia solution. The obtained solution was homogenized with a magnetic stirrer at around 85 °C. After 3 h, the mixture became gel which was placed on a hot plate at around 280–350 °C to evaporate the remaining solvent and the precursor material was formed. A Muffle furnace was used to heat the precursor material at 1000 °C for 5 h and $BaFe_{11.8}Bi_{0.1}Al_{0.1}O_{19}$ powder was formed.

2.2 Synthesis method of polyaniline (PANI)

The synthesis of PANI was done via oxidative polymerization method. In this process, 91.15 mL of hydrochloric acid (0.1 M) was placed under rotation at 0 °C in an ice bath, and then 23.282 mL of aniline monomer was added gradually. After 30 min, 40.47 gm of Ammonia persulphate (APS) dissolved in water was gradually added. The set was stirred for 6 h to permit the reaction to take place. Distilled water was added to dilute and the resulting solution was filtered and washed with methanol and distilled water then put in oven at 60 °C to dry. After 2 days, PANI powder with green color was obtained.

2.3 Synthesis method of $BaFe_{11.8}Bi_{0.1}Al_{0.1}O_{19}$-PANI composite

Mechanical blending process was used to blend the previous prepared samples using a mortar and pestle. The composites were obtained according to the ratios (hexaferrite: PANI) 1:1, 1:1.5 and 1:2 (Table 1).

3 Characterization techniques

Bruker AXS D8 advance diffractometer using Cu-K α radiation in the range 20°–80° operating at 35 mA and 40 kV with step size 0.02° was utilized to record X-ray diffraction patterns and study structural and phase analysis of prepared samples. FTIR spectrometer (Nicolet FTIR interferometer IR prestige-21 (model-8400S)) in the range 4000–400 cm^{-1} was used to carry out different functional groups and characteristic signature of the prepared samples. Analysis of the morphology and composition of the prepared samples was examined using FESEM and EDXS (FEI Nova NanoSEM 450 FESEM). Band gap of the prepared samples was carried out using UV–Vis-NIR Spectrometer (Varian, Cary 5000) in the wavelength range 200–780 nm.

4 Results and discussions

4.1 X-ray diffraction (XRD) analysis

The crystal structure of $BaFe_{11.8}Bi_{0.1}Al_{0.1}O_{19}$-PANI nanocomposites was studied using X-ray diffraction. XRD patterns of prepared samples are given in Fig. 1. The observed peaks in this figure was indexed using 39-1433 as JCPDS card [25] which correspond to the standard XRD patterns of M-Type barium hexaferrite with *P63/mmc* as space group. It can be observed that the reflection planes of $BaFe_{11.8}Bi_{0.1}Al_{0.1}O_{19}$ perfectly match to that of M-type Barium hexaferrite. The absence of second phase confirms the single crystal phase of $BaFe_{11.8}Bi_{0.1}Al_{0.1}O_{19}$ which indicates that Al^{3+} and Bi^{3+} ions occupied perfectly crystallographic sites of Fe^{3+}

Table 1 Samples code and composition of $BaFe_{11.8}Bi_{0.1}Al_{0.1}O_{19}$-PANI

Sample code	Ratio
HP1	1:1
HP2	1:1.5
HP3	1:2

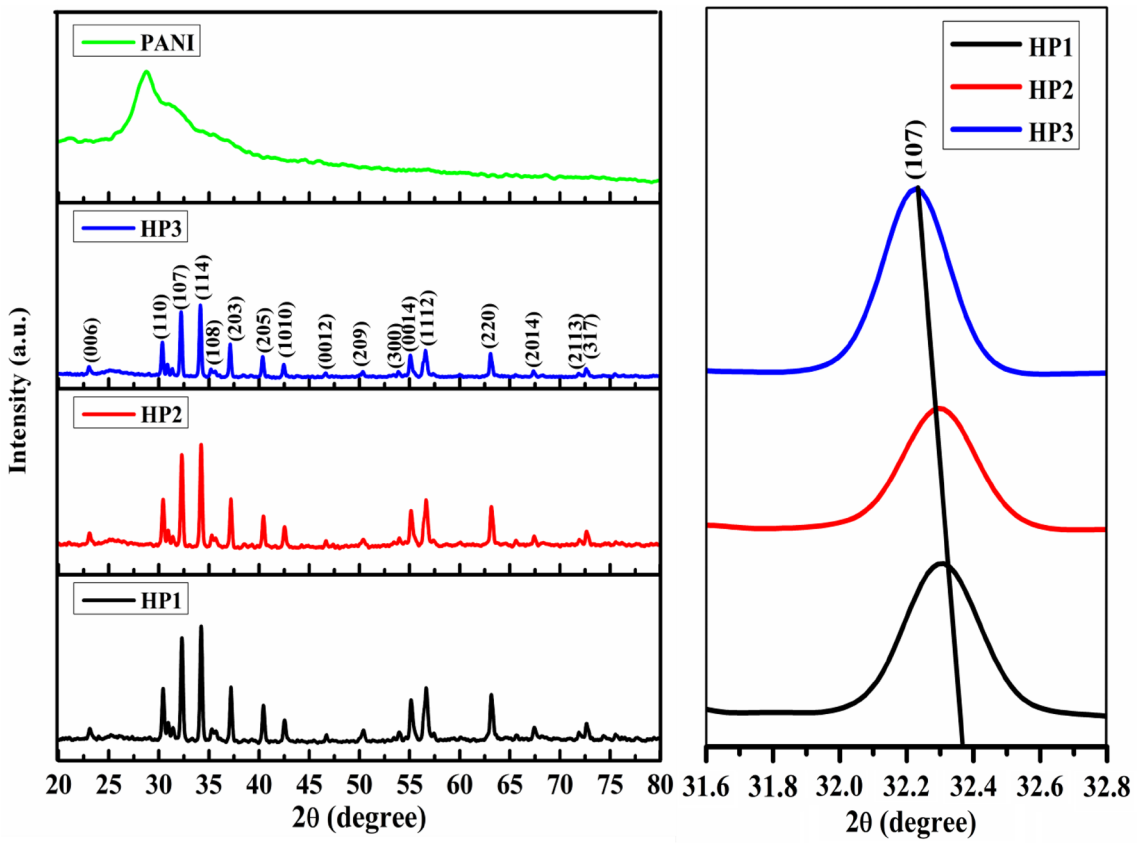

Fig. 1 XRD patterns of PANI and $BaFe_{11.8}Bi_{0.1}Al_{0.1}O_{19}$-PANI composite

ions. Generally in M-type hexaferrite, the second phase (α -Fe_2O_3) appears at around 2 $\theta = 33.13$ and correspond to (103) diffraction plane. From Fig. 1, the presence of PANI in the composite is materialized by the large peak observed at around 2 $\theta = 25.12–25.46$; this is supported by Luo and Yuan [26, 27]. Rietveld refinement of the crystal structure of $BaFe_{11.8}Bi_{0.1}Al_{0.1}O_{19}$ was performed using FULLPROF suite package. The diffraction peaks were modeled with Thompson-Cox-Hastings pseudo-Voigt * Axial divergence asymmetry function and linear interpolation method was used to model the background. During the refinement, parameters such as occupancy of all atoms, background, atomic positions, unit cell, half-width and zero position were varying throughout the process. This refinement confirmed that the observed peaks in XRD patterns match with those of M-type hexaferrite (Fig. 2). The quality of refinement is justified by reliability factors (R_p, R_{wp}, R_{exp}, χ^2 and GoF) given in Table 2. GoF (Good of fit) has been found to be between 1.6 and 1.8. Crystallite size (D), lattice parameters (a and c) and volume of unit cell (V) have been calculated using the following formulae and tabulated in Table 2 [28]:

$$\frac{1}{d_{hkl}^2} = \frac{4}{3}\left(\frac{h^2 + hk + k^2}{a^2}\right) + \frac{l^2}{c^2} \quad (1)$$

$$V_{cell} = \frac{\sqrt{3}}{2}a^2c \quad (2)$$

$$D = \frac{0.9\lambda}{\beta \cos\theta} \quad (3)$$

where d_{hkl} refers to d-spacing, hkl are the miller indices, $\lambda = 1.54056$ Å is the wavelength of incident X-ray, β is full width at half maxima (in radian), θ is the Bragg angle. The crystallite size of prepared composite were found to be between 37 and 41 nm while lattice parameters a, c and $Vcell$ were found to be in the range 5.86–5.89 Å, 23.11–23.17 Å and 689.37–694.56 $Å^3$. It was observed that a, c and Vcell increase with amount of PANI. This can be due to the fact that after adding PANI, the crystal structure of $BaFe_{11.8}Bi_{0.1}Al_{0.1}O_{19}$ has undergone some distortions. This distortion (stretching) of the structure can be justified by the shift of diffraction angle (2θ) toward small values (Fig. 1). Bulk density (d_m) of sample was estimated and was

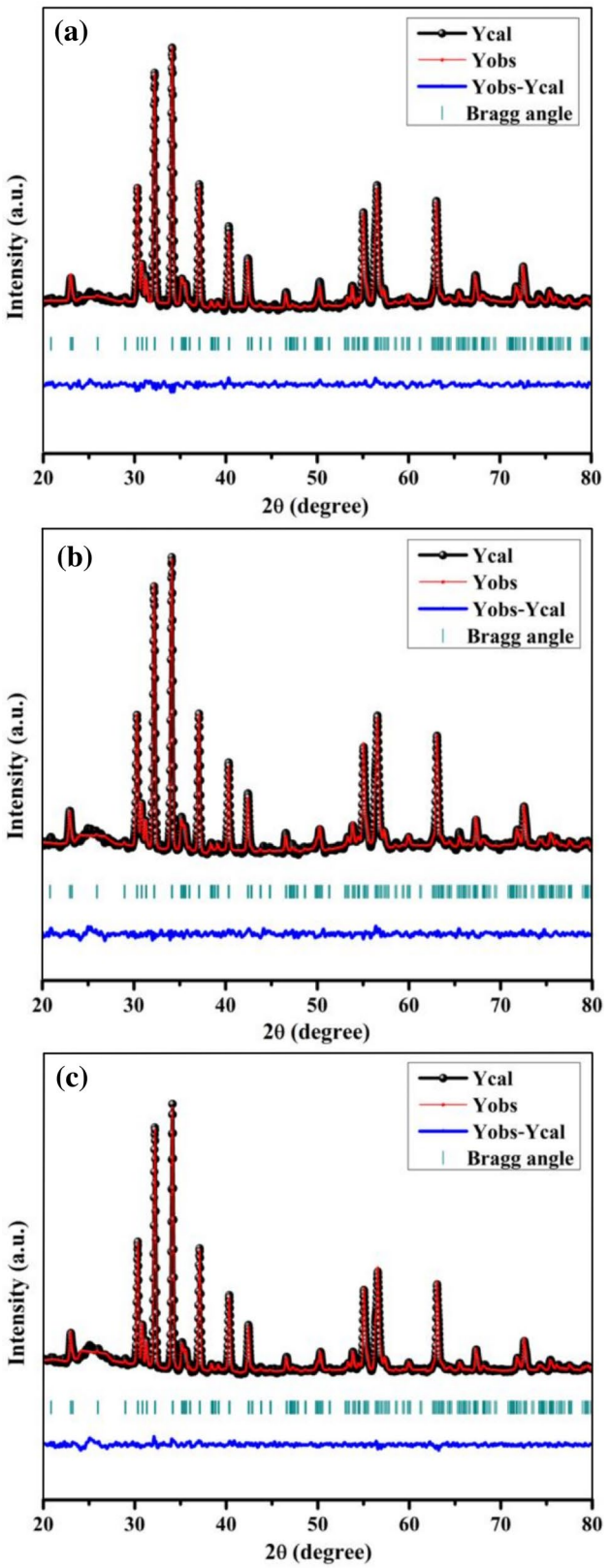

Fig. 2 Rietveld refinement of $BaFe_{11.8}Bi_{0.1}Al_{0.1}O_{19}$-PANI composite **a** HP1, **b** HP2 and **c** HP3

Table 2 Structural parameters and reliability factors

X	HP1	HP2	HP3
β(°)	0.224	0.225	0.194
Crystallite size (D) nm	37.108	35.307	40.949
Lattice parameter (a) Å	5.868	5.872	5.884
Lattice parameter (c) Å	23.114	23.114	23.163
Volume of unite cell (V) $Å^3$	689.37	690.122	694.55
Bulk density (d_m) g/cm^3	1.111	1.175	1.094
R_{bragg}	5.57	6.72	5.13
R_P	13.2	14.0	12.6
R_{wp}	21.7	22.9	20.7
R_{exp}	12.1	14.2	12.4
χ^2	3.229	2.608	2.792
GoF	1.8	1.6	1.7

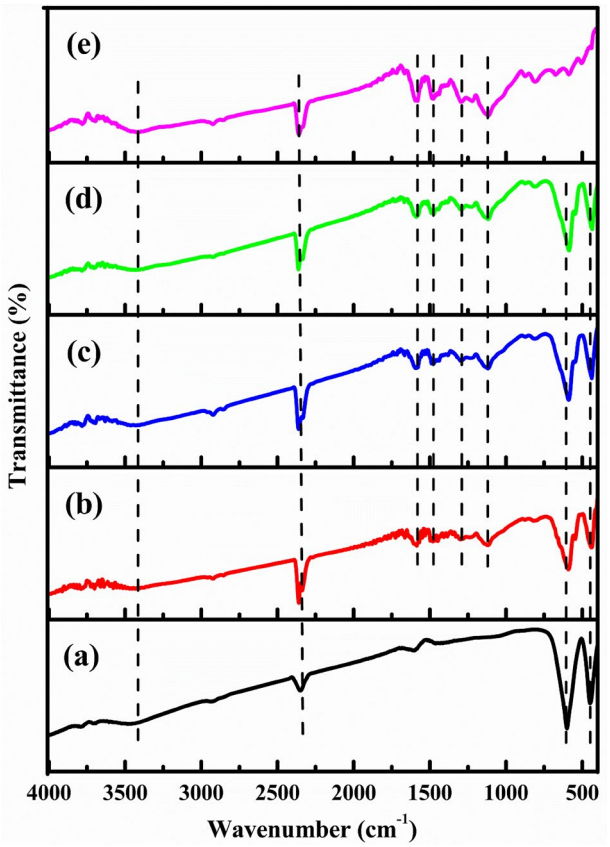

Fig. 3 FTIR spectra of **a** $BaFe_{11.8}Bi_{0.1}Al_{0.1}O_{19}$, **b** HP1, **c** HP2, **d** HP3 and **e** PANI

found to be between 1.09 and 1.18 g/cm^3. These values are very small compared to the bulk density of M-type barium hexaferrite ($BaFe_{12}O_{19}$) which is around 3.23 g/cm^3 [5]. This

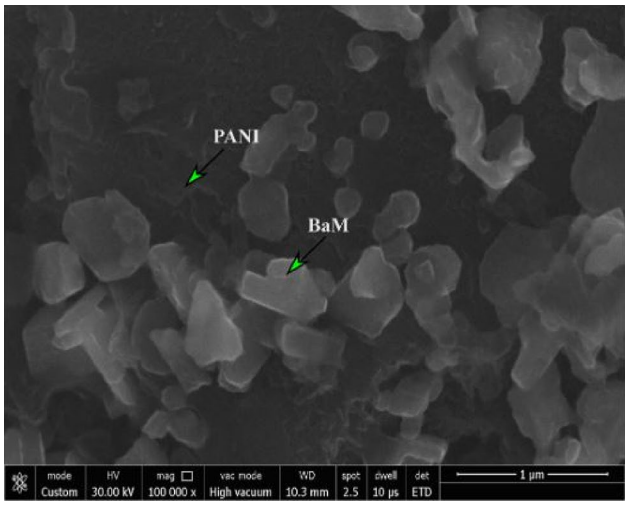

Fig. 4 FESEM micrographs of $BaFe_{11.8}Bi_{0.1}Al_{0.1}O_{19}$-PANI composite

may be due to the fact that PANI is less dense than M-type hexaferrite material.

4.2 Fourier transform-infrared (FTIR) analysis

FTIR spectroscopy was used to determine functional groups and chemical residual in the prepared samples. For analysis, thin pellets of KBr with the prepared samples in the ratio 10:1 respectively have been made. Figure 3 shows FTIR spectra of $BaFe_{11.8}Bi_{0.1}Al_{0.1}O_{19}$, PANI and $BaFe_{11.8}Bi_{0.1}Al_{0.1}O_{19}$-PANI composites recorded in the wavenumber range 400–4000 cm^{-1}. FTIR spectrum of PANI is given in Fig. 3e and its characteristic absorption peaks were found at around 804 cm^{-1} (out-of plane deformation vibration of benzene ring), 1123 and 1601 cm^{-1} (vibration band of N=Q=N) indicating the formation of PANI, 1297 cm^{-1} (N–H bending band of benzenoid rings) and 1486 cm^{-1} (C=N stretching of quinoid ring) [29–34]. Figure 3b–d shows FTIR spectra for HP1, HP2 and HP3 respectively. In these figures, it can be noticed that all characteristic peaks of PANI appearing in 1000–1600 cm^{-1} were present in HP1, HP2 and HP3 spectra but were not present in the spectrum of $BaFe_{11.8}Bi_{0.1}Al_{0.1}O_{19}$ which indicate the presence of both $BaFe_{11.8}Bi_{0.1}Al_{0.1}O_{19}$ particles and PANI in HP1, HP2 and HP3 samples. The characteristic peaks of $BaFe_{11.8}Bi_{0.1}Al_{0.1}O_{19}$ are defined by Fe–O bond vibration at 442 and 587 cm^{-1} (Fig. 3a) [25]. The intensity of these two peaks is higher in the spectrum of $BaFe_{11.8}Bi_{0.1}Al_{0.1}O_{19}$ compared to those of composites indicating that the composites show less absorbance than $BaFe_{11.8}Bi_{0.1}Al_{0.1}O_{19}$. The peak observed at 2356 cm^{-1} refers to the presence of CO_2 in the sample which was absorbed from the atmosphere and the wide band at 3429 cm^{-1} refers to the vibration of –OH group [35].

4.3 Morphological analysis

FESEM micrograph of $BaFe_{11.8}Bi_{0.1}Al_{0.1}O_{19}$-PANI composite (HP1) is given in Fig. 4. In this image, the presence of PANI and $BaFe_{11.8}Bi_{0.1}Al_{0.1}O_{19}$ (BaM) particles were observed and the particles size of BaM was found to be in the range of 25–50 nm. EDX analysis (Fig. 5) shows that all chemical elements of the composites of $BaFe_{11.8}Bi_{0.1}Al_{0.1}O_{19}$ and PANI are presents which support the homogenous distribution and results revealed by XRD analysis.

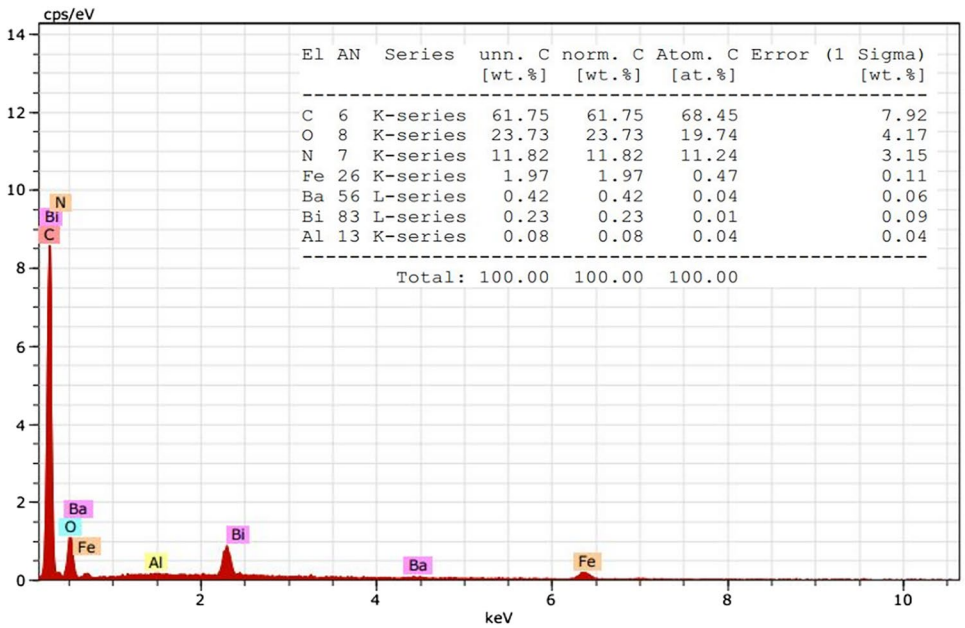

Fig. 5 EDX spectra of $BaFe_{11.8}Bi_{0.1}Al_{0.1}O_{19}$-PANI composite

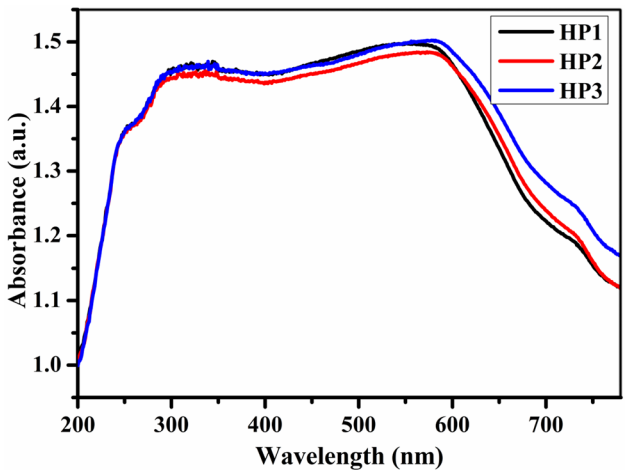

Fig. 6 Absorbance of $BaFe_{11.8}Bi_{0.1}Al_{0.1}O_{19}$-PANI composite

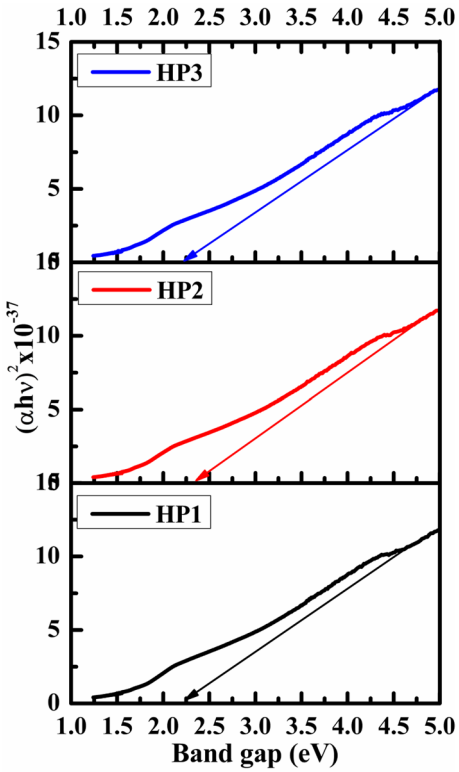

Fig. 7 Optical band gap of $BaFe_{11.8}Bi_{0.1}Al_{0.1}O_{19}$-PANI composite

4.4 Optical analysis

UV–vis spectroscopy was employed to examine optical properties of the $BaFe_{11.8}Bi_{0.1}Al_{0.1}O_{19}$-PANI composite. Figure 6 exhibits the absorbance spectra of prepared sample in the range 200–780 nm. According to the literature, PANI presents two characteristic absorption bands in UV–vis spectrum especially at around 336 nm and 600 nm which are assigned to $\pi - \pi^*$ transition phenyl ring and $n - \pi^*$ transition benzenoid to quinoid respectively [32, 36]. In the present case, the UV–vis spectra are also showing two large absorption peaks indicating the presence of PANI.

The two absorption bands were found at around 323 nm and 580 nm for HP1, at 323 nm and 584 nm for HP2 and at 323 nm and 585 nm for HP3. Compared to the absorption bands of PANI, it was noticed that peaks of HP1, HP2 and HP3 show blue shift (hypsochromic shift) which can be due to the interaction between oxygen in hexaferrite particles and –NH in PANI [33]. These absorption bands indicate the passage from valence band to the conduction band. The transition requires an energy defined by the band gap energy (E_g) calculated from the following equation [37, 38]:

$$(\alpha hv)^2 = B\left(hv - E_g\right) \tag{4}$$

where A is a constant, E_g is the band gap energy and h is the Planck's constant. Figure 7 shows Eg plots of prepared sample. After an extrapolation of linear part of the curve of $(\alpha hv)^2$ against E_g, band gap energies of prepared samples have been estimated and were found to be 2.24, 2.36 and 2.21 eV for HP1, HP2 and HP3 respectively. For all the samples the values of E_g were found to be lesser than 3.18 eV [39]. It can be noticed that the band gap values and crystallite size vary inversely that means higher the crystallite size smaller the band gap. This can be explained by quantum confinement effects [6].

5 Conclusion

$BaFe_{11.8}Bi_{0.1}Al_{0.1}O_{19}$-PANI nanocomposites have been prepared using mechanical blending after preparing $BaFe_{11.8}Bi_{0.1}Al_{0.1}O_{19}$ and PANI by sol gel auto combustion technique and oxidative polymerization respectively. XRD analysis and Rietveld refinement revealed the formation of single phase of $BaFe_{11.8}Bi_{0.1}Al_{0.1}O_{19}$ incorporated in PANI matrix. The presence of PANI was observed at around 25°. FTIR analysis showed the characteristic functional groups of both PANI and M-type hexaferrite describing the composite nature of HP1, HP2 and HP3. Band gap was estimated by UV–vis analysis and values were found to be between 2.21 and 2.36 eV.

Acknowledgements The authors thank Material Research Centre (MRC), Malaviya National Institute of Technology (MNIT), Jaipur, India for FESEM and EDX analysis, Sophisticated Test and Instrumentation

and Centre (STIC), Cochin University of Science and Technology, Kerala, India for UV–Vis-NIR Spectrophotometer characterization.

Compliance with ethical standards

Conflict of interest The authors declare that they have no conflict of interest.

References

1. Auwal IA, Baykal A, Güngüneş H, Shirsath SE (2016) Structural investigation and hyperfine interactions of $BaBi_xLa_xFe_{12-2x}O_{19}$ ($0.0 \le x \le 0.5$) hexaferrites. Ceram Int 42:3380–3387
2. Ashraf GA, Zhang L, Abbas W, Murtaza G (2018) Synthesis and characterizations of Al-Sm substituted Ba-Sr M-type hexagonal ferrite nanoparticles via sol–gel route. Ceram Int 44:18678–18685
3. Mousavi Ghahfarokhi SE, Ranjbar F, Zargar Shoushtari M (2014) A study of the properties of $SrFe_{12-x}Co_xO_{19}$ nanoparticles. J Magn Magn Mater 349:80–87
4. Kaur T, Kumar S, Hamid B, Bhat BH, Want B, Srivastava AK (2015) Effect on dielectric, magnetic, optical and structural properties of Nd–Co substituted barium hexaferrite nanoparticles. Appl Phys A 119:1531–1540
5. Tchouank Tekou Carol T, Mohammed J, Hafeez HY, Bhat BH, Godara SK, Srivastava AK (2019) Structural, dielectric, and magneto-optical properties of Al-Cr substituted M-type barium hexaferrite. Phys Status Solidi A 216:1800928
6. Baykal A, Auwal IA, Güner S, Sözeri H (2017) Magnetic and optical properties of Zn^{2+} ion substituted barium hexaferrites. J Magn Magn Mater 430:29–35
7. Ibraheam AS, Al-Douri Y, Mohammed AS, Prakash D, Hashim U, Verma KD (2015) Electrical, optical and structural properties of $Cu_2Zn_{0.8}Cd_{0.2}SnS_4$ quinternary alloy nanostructures synthesized by spin coating technique. Int J Electrochem Sci 10:9863–9876
8. Gurunathan K, Amalnerkar DP, Trivedi DC (2003) Synthesis and characterization of conducting polymer composite (PAn/TiO_2) for cathode material in rechargeable battery. Mater Lett 57:1642–1648
9. Deshpande NG, Gudage YG, Sharma R, Vyas JC, Kim JB, Lee YP (2009) Studies on tin oxide-intercalated polyaniline nanocomposite for ammonia gas sensing applications. Sens Actuators B Chem 138:76–84
10. Peng C, Zhang S, Jewell D, Chen GZ (2008) Carbon nanotube and conducting polymer composites for supercapacitors. Prog Nat Sci 18:777–788
11. Olad A, Barati M, Shirmohammadi H (2011) Conductivity and anticorrosion performance of polyaniline/zinc composites: investigation of zinc particle size and distribution effect. Prog Org Coat 72:599–604
12. Sathiyanarayanan S, Karpakam V, Kamaraj K, Muthukrishnan S, Venkatachari G (2010) Sulphonate doped polyaniline containing coatings for corrosion protection of iron. Surf Coat Technol 204:1426–1431
13. Aksit AC, Onar N, Ebeoglugil MF, Birlik I, Celik E, Ozdemir I (2009) Electromagnetic and electrical properties of coated cotton fabric with barium ferrite doped polyaniline film. J Appl Polym 113:358–366
14. Yuan CL, Hong YS (2010) Microwave adsorption of core–shell structure polyaniline/$SrFe_{12}O_{19}$ composites. J Mater Sci 45:3470–3476
15. Birsöz B, Baykal A, Sözeri H, Toprak MS (2010) Synthesis and characterization of polypyrrole-$BaFe_{12}O_{19}$ nanocomposite. J Alloys Compd 493:481–485
16. Tyagi S, Baskey HB, Agarwala RC, Agarwala V, Shami TC (2011) Development of hard/soft ferrite nanocomposite for enhanced microwave absorption. Ceram Int 37:2631–2641
17. Hojjati-Najafabadi A, Ghasemi A, Mozaffarinia R (2017) Magneto-electric features of $BaFe_{9.5}Al_{1.5}CrO_{19}$–$CaCu_3Ti_4O_{12}$ nanocomposites. Ceram Int 43:244–249
18. Zhao WY, Wei P, Cheng HB, Tang XF, Zhang QJ (2007) FTIR spectra, lattice shrinkage, and magnetic properties of CoTi-substituted M-type barium hexaferrite nanoparticles. J Am Ceram Soc 90:2095–2103
19. Ibraheam AS, Al-Douri Y, Hashim U (2015) Effect of copper concentration on characterization of $Cu_2Zn_{0.8}Cd_{0.2}SnS_4$ pentrary alloy nanostructures. Appl Mech Mater 754–755:1115–1119
20. Ibraheam AS, Al-Douri Y, Hashim U, Al-Mufti MW (2015) Characterization of $Cu_2Zn_{1-x}Cd_xSnS_4$ nanostructures. Adv Mater Res 1109:171–175
21. Ibraheam AS, Al-Douri Y, Al-Fhdawi JMS, Al-Jumaili HS, Verma KD, Hashim U, Ayub RM, Rahim Ruslinda A, Md Arshad MK, Reshak AH, Hamid Abd (2016) Structural, optical and electrical properties of $Cu_2Zn_{1-x}Cd_xSnS_4$ quinternary alloys nanostructures deposited on porous silicon. Microsyst Technol 22:2893–2900
22. Ibraheam AS, Al-Douri Y, Hashim U (2015) Effect of copper concentration on the optical properties of $Cu_2Zn_{0.8}Cd_{0.2}SnS_4$ pentrary alloy nanostructures. Adv Mater Res 1115:373–377
23. Ibraheam AS, Al-Douri Y, Hashim U, Ghezzar MR, Addou A, Ahmed WK (2015) Cadmium effect on optical properties of $Cu_2Zn_{1-x}Cd_xSnS_4$ quinternary alloys nanostructures. Sol Energy 114:39–50
24. Ibraheam AS, Al-Douri Y, Hashim U, Ameri M, Bouhemadou A, Khenata R (2017) Structural, optical and electrical investigations of $Cu_2Zn_{1-x}Cd_xSnS_4$/Si quinternary alloy nanostructures synthesized by spin coating technique. Microsyst Technol 23:2223–2232
25. Tchouank Tekou Carol T, Sharma J, Mohammed J, Kumar S, Srivastava AK (2017) Effect of temperature on the magnetic properties of nano-sized M-type barium hexagonal ferrites. AIP Conf Proc 1860:020008
26. Luo J, Shen P, Yao W, Jiang C, Xu J (2016) Synthesis, characterization, and microwave absorption properties of reduced graphene oxide/strontium ferrite/polyaniline nanocomposites. Nanoscale Res Lett 11:141
27. Yuan CL (2016) Polyaniline coated magnetic particles of manganese titanium substituted strontium hexaferrites composites as microwave absorbers. J Mater Sci Mater Electron 27:4908–4912
28. Tchouank Tekou Carol T, Mohammed J, Basandrai D, Godara SK, Bhadu GR, Mishra S, Aggarwal N, Narang SB, Srivastava AK (2020) X-band shielding of electromagnetic interference (EMI) by Co_2Y barium hexaferrite, bismuth copper titanate (BCTO), and polyaniline (PANI) composite. J Magn Magn Mater 501:166433
29. Ben Ghzaiel T, Dhaoui W, Schoenstein F, Talbot P, Mazaleyrat F (2017) Substitution effect of Me=Al, Bi, Cr and Mn to the microwave properties of polyaniline/$BaMeFe_{11}O_{19}$ for absorbing electromagnetic waves. J Alloys Compd 692:774–786
30. Kuo HM, Hsui TF, Tuo YS, Yuan CL (2012) Microwave adsorption of core-shell structured $Sr(MnTi)_xFe_{12-2x}O_{19}$/PANI composites. J Mater Sci 47:2264–2270
31. Saini P, Choudhary V, Singh BP, Mathur RB, Dhawan SK (2009) Polyaniline-MWCNT nanocomposites for microwave absorption and EMI shielding. Mater Chem Phys 113:919–926
32. Deng J, He C, Peng Y, Wang J, Long X, Li P, Chan ASC (2003) Magnetic and conductive Fe_3O_4– polyaniline nanoparticles with core–shell structure. Synth Met 139:295–301

33. Mostafaei A, Zolriasatein A (2012) Materials international synthesis and characterization of conducting polyaniline nanocomposites containing ZnO nanorods. Prog Nat Sci Mater Int 22:273–280
34. Ting TH, Yu RP, Jau YN (2011) Synthesis and microwave absorption characteristics of polyaniline/NiZn ferrite composites in 2–40 GHz. Mater Chem Phys 126:364–368
35. Tchouank Tekou Carol T, Mohammed J, Bhat BH, Mishra S, Godara SK, Srivastava AK (2019) Effect of Cr–Bi substitution on the structural, optical, electrical and magnetic properties of strontium hexaferrites. Phys B Condens Matter 575:411681
36. Khanna PK, Singh N, Charan S, Viswanath AK (2005) Synthesis of Ag/polyaniline nanocomposite via an in situ photo-redox mechanism. Mater Chem Phys 92:214–219
37. Mohammed J, Suleiman AB, Hafeez HY, Tchouank Tekou Carol T, Sharma J, Bhadu GR, Godara SK, Srivastava AK (2018) Effect of heat-treatment on the magnetic and optical properties of $Sr_{0.7}Al_{0.3}Fe_{11.4}Mn_{0.6}O_{1.9}$. Mater Res Express 5:086106
38. Tchouank Tekou Carol T, Mohammed J, Srivastava AK (2019) Effect of calcination temperature on the structural, dielectric and optical properties of nano-sized M-type barium hexaferrites. Mater Today Proc 18:566–574
39. Karmakar M, Mondal B, Pal M, Mukherjee K (2014) Acetone and ethanol sensing of barium hexaferrite particles: a case study considering the possibilities of non-conventional hexaferrite sensor. Sens Actuators B hem. 190:627–633